01

Phase-field model of growth and dissolution of stoichiometric phase in binary solution

© S.A. Korobeynikov,[1,2] V.G. Lebedev,[2] V.I. Ladyanov[2]

[1] Udmurt State University,
426034 Izhevsk, Russia
[2] Udmurt Federal Research Center, Ural Branch Russian Academy of Sciences,
426067 Izhevsk, Russia
e-mail: sa.korobeynikov@yandex.ru

Received April 4, 2024
Revised July 1, 2024
Accepted July 2, 2024

The phase-field approach for describing the growth and dissolution of a phase of constant composition in a binary solution is considered. The relaxation equations for the phase field and impurity concentration in the phase of variable composition, taking into account the thermodynamic properties of compounds, are derived from the condition of non-decreasing Gibbs energy. It is demonstrated that the equations derived from the principles of nonequilibrium thermodynamics and the law of conservation of matter in volume imply the existence of two mechanisms of growth and dissolution of stoichiometries. The model permits the use of an arbitrary binary system with stoichiometries. For purposes of verification, the Si−Ti binary system, described by the experimentally calculated Gibbs energies of the phases, has been employed. A one-dimensional numerical simulation of the phase transition process under different initial conditions has been conducted, exhibiting qualitative agreement with the anticipated behaviour of the melting−solidification processes.

Keywords: binary solution, Gibbs energy, melting, solidification, phase transition.

DOI: 10.61011/TP.2024.10.59352.110-24

Introduction

The development of novel and promising materials based on composites [1] often implies dealing with inclusions of constant composition (so-called stoichiometric phases or compounds) that provide the necessary physical and chemical material properties. Such compounds [2] include carbides, nitrides, oxides, and intermetallic compounds. Stoichiometric phases are also widespread in the mass metallurgical production of steel and iron. Iron carbide (cementite) and graphite inclusions present in them [3] are phases of constant composition. The unique mechanical properties of numerous high-alloy steels are the result of formation of carbides and nitrides by alloying components [4]. Experimental studies into the strength characteristics of the Al−Ni binary system [5] revealed the formation of the Al_3Ni stoichiometric phase in the interdendritic region, which has a significant effect on the ultimate tensile strength and tensile yield strength. Another issue related to the influence of phases of constant composition is the growth of Cu_6Sn_5 in soldered copper contacts [6,7]. Extended non-monotonic relaxation of viscosity near the liquidus line, which bounds the two-phase region of liquid and the Al_3Y stoichiometry, was observed in the study focused on measurement of the Al−Y melt viscosity [8].

The prediction of formation of compounds in computer packages for casting simulation (similar to [9]) is a relevant problem that has not been quite resolved yet: the issue lies in incomplete theoretical understanding of this process.

The thermodynamic peculiarity of phases of constant composition is in the mathematical description of their Gibbs energy as a function of temperature only [10], which precludes one from finding the chemical potential of a phase as a derivative with respect to the mole fraction (concentration) of an impurity. Nevertheless, chemical potential is crucial to understanding the phase equilibrium and determines the course of relaxation processes in multicomponent systems. One of the previously proposed approaches to solving the problem of uncertainty of chemical potential consists in substituting the Gibbs energy of a phase of constant composition by a parabola with its parameters determined from the required dynamics [11]. Although this approach allows one to characterize the processes of growth and dissolution, it does not always provide an accurate description of the actual behavior of the system, since the choice of approximating parabolas is fairly arbitrary.

It is evident that the problem of characterizing the kinetics of growth and dissolution of stoichiometric phases is relevant to the prediction of microstructure of multicomponent systems used in modern metallurgical production. One of the key steps toward solving the indicated problem is to obtain a system of equations that characterize the processes of interaction of phases of variable composition and stoichiometries „as is“ without changing the type of Gibbs energy and with account for thermodynamic uncertainty of the chemical potential of the stoichiometries. To gain a better understanding of the physics of the process, we limit ourselves to the two-phase interaction in a binary

system, simplifying the analysis of the resulting system of equations. Thus, the aim of the present study is to derive a system of equations for the kinetics of growth and dissolution of stoichiometric phases in the two-phase case with account for their thermodynamic features and verify the obtained model via numerical simulations for a real binary system.

It is demonstrated below that if we rely on nonequilibrium thermodynamics, a model close to the one obtained in [12] follows from the principle of Gibbs energy reduction for a two-phase binary system and with account for the law of conservation of impurity in volume. A significant step up from the indicated model is the presence of a thermodynamically consistent diffusion equation for the mole fraction in the liquid phase, which brings the present model closer to the phase field model for the interaction of two phases of variable composition [13]. It is demonstrated that the model operates correctly with nonzero mole fractions in phases of constant composition, which was not investigated in [12]. The obtained model is examined numerically by comparing the dynamics of the phase field profiles and the impurity concentration in the phase of variable composition (liquid phase) in the case of solidification proceeding via diffusion-controlled and kinetic mechanisms. The change in the total Gibbs energy of the system and the conservation of matter in the simulated volume are estimated. Simulations are also performed for different initial values of the mole fraction in the liquid phase, and the correspondence of dynamics to the expected physical processes is demonstrated.

1. Dynamics equations

Let us consider the problem of interaction between a phase of constant composition (stoichiometry or solid phase) and a phase of variable composition (liquid phase) in a two-component (binary) system in the isothermal case, which is commonly understood as a scenario where temperature is an external parameter of the system that remains constant in space, but possibly varies with time.

Let us introduce scalar field $\varphi(\mathbf{r}, t)$ that characterizes unambiguously the state of matter at a point in space. In the stoichiometry (S) volume, the phase field has constant value $\varphi = 1$; in the liquid phase (L) volume, the value is $\varphi = 0$. In the region of phase transition, φ varies smoothly but rapidly from 0 to 1, forming a diffuse boundary. Scalar field $x_L(\mathbf{r}, t)$ characterizes the mole fraction of impurity in the liquid phase; the mole fraction of impurity in the solid phase is constant and equal to x_S.

Let us examine the Gibbs energy functional for the above system with the volume change in phase transition being neglected:

$$G = \int_V \Big[p(\varphi) G^S(T) + \big(1 - p(\varphi)\big) G^L(x_L, T) + W g(\varphi) + \frac{\sigma^2}{2} (\nabla\varphi)^2 \Big] \mathrm{d}V, \qquad (1)$$

where $G^S(T)$ and $G^L(x_L, T)$ are the equilibrium bulk Gibbs energy densities of the stoichiometric and liquid phases, respectively; $p(\varphi)$ is the interpolation function that ensures phase stability; $g(\varphi)$ is the „double-well" potential that constrains spontaneous transitions between phases; $(\nabla\varphi)^2$ is the contribution of the interface surface between phases associated with the diffuse boundary; W is the energy barrier height; and σ is the kinetic coefficient related to surface energy. In what follows, the explicit dependence on φ for $p(\varphi)$ and $g(\varphi)$ and the dependence on temperature T and x_L for $G^L(x_L, T)$ and $G^S(T)$ are omitted for brevity.

According to Kessler [14], functions p and g may be chosen fairly arbitrarily, but must satisfy mandatory conditions

$$p(0) = 0,\ p(1) = 1,\ p(1-\varphi) = 1 - p(\varphi),\ p'(0) = p'(1) = 0,$$

$$g(0) = g(1) = g'(0) = g'(1) = 0, \quad g''(\varphi) < 0,$$

where $(')$ denotes a derivative with respect to the argument. The following expressions are used in the present study:

$$p(\varphi) = \varphi^3(10 - 15\varphi + 6\varphi^2), \quad g(\varphi) = \varphi^2(1 - \varphi)^2.$$

We find the time derivative of the total Gibbs energy by transforming the term with mixed derivative $\sigma^2 \nabla\varphi(\dot{\nabla}\varphi)$ in accordance with the Gauss theorem under the assumption of constancy of φ at the boundaries of the system volume. The dot accent $(\dot{})$ denotes a partial time derivative.

Having grouped the terms, we then obtain an expression for the time derivative of the Gibbs energy:

$$\frac{\mathrm{d}G}{\mathrm{d}t} = \int_V \Big[\dot{\varphi} \left(-\sigma^2 \nabla^2 \varphi + W g' + p'(G^S - G^L) \right) + (1 - p)\mu^L \dot{x}_L \Big] \mathrm{d}V, \qquad (2)$$

where

$$\mu^L = \mu^L(x_L) = \frac{\partial G^L}{\partial x_L}.$$

Let us write down the law of conservation of impurity in the studied system. The fraction of impurity in the liquid phase is not conserved due to the processes of impurity exchange between phases. However, the total amount of impurity in the solution is conserved. Therefore, we take averaged concentration in volume $\langle x \rangle = p x_S + (1 - p) x_L$ as the conserved quantity. The law of conservation is then written as

$$\frac{\partial}{\partial t} \langle x \rangle = (1 - p)\dot{x}_L + (x_S - x_L) p' \dot{\varphi} = -\nabla \cdot \mathbf{J}_D, \qquad (3)$$

where $\mathbf{J}_D$ is the diffusion flux. Next, we derive an expression for $(1 - p)\dot{x}_L$ from relation (3) and insert it into (2). Having transformed the $-\mu^L \nabla \cdot \mathbf{J}_D$ expression in accordance with the Gauss theorem under the assumption of

zero diffusion flux at the boundaries of the system volume and grouped the terms, we present derivative (2) as

$$\frac{\mathrm{d}G}{\mathrm{d}t}=\int\limits_V\Big[\dot\varphi\Big(-\sigma^2\nabla^2\varphi+Wg'+p'\big(G^S-G^L-(x_S-x_L)\mu^L\big)\Big)+\mathbf{J}_D\nabla\mu^L\Big]\mathrm{d}V. \tag{4}$$

The following is the simplest choice of a system of equations ensuring that the Gibbs energy does not increase (in accordance with the principles of irreversible thermodynamics [15]):

$$\begin{cases}\dot\varphi=-M_\varphi\big[-\sigma^2\nabla^2\varphi+Wg'+p'(G^S-G^L-(x_S-x_L)\mu^L)\big],\\ \mathbf{J}_D=-M_D\,\nabla\mu^L,\end{cases} \tag{5}$$

where $M_\varphi\geq 0$ is the phase field mobility and $M_D\geq 0$ is the diffusion mobility.

It is evident that the diffusion flux should be localized in the liquid phase; therefore, relying on the positive definiteness of mobility, we perform substitution $M_D=(1-p)M_F$ and obtain

$$\mathbf{J}_D=-(1-p)M_F\nabla\mu^L.$$

At $T=\mathrm{const}$, a connection with the Fick's law in the liquid phase becomes evident:

$$\mathbf{J}_D=-(1-p)M_F\nabla\mu^L=-(1-p)M_F\frac{\partial\mu^L}{\partial x_L}\nabla x_L=-(1-p)D\nabla x_L.$$

Having inserted the obtained expression for flux $\mathbf{J}_D$ into conservation law (3) and derived an expression for $(1-p)\dot x_L$, we obtain a system of equations for the dynamics of the phase field and the mole fraction of impurity in the liquid phase:

$$\begin{cases}\dot\varphi=M_\varphi\big[\sigma^2\nabla^2\varphi-Wg'-p'\big(G^S-G^L-(x_S-x_L)\mu^L\big)\big],\\ (1-p)\dot x_L=-(x_S-x_L)p'\dot\varphi+\nabla\big[(1-p)M_F\nabla\mu^L\big].\end{cases} \tag{6}$$

2. Analysis of the obtained equations

Let us analyze the obtained equation for the phase field. Consider a graphical interpretation of the Gibbs phase equilibrium between a stoichiometry and a phase of variable composition. The condition for phase equilibrium of two phases of variable composition is the presence of a common tangent in the coordinates of concentration and Gibbs energy. This condition corresponds to the equality of chemical potentials (the value of the first derivative at a point as the slope of the tangent). Since it is impossible to draw a tangent to the stoichiometric phase in the indicated coordinates, the only option that ensures „coherence" of Gibbs energies is a tangent to the phase of variable composition passing through the point of Gibbs

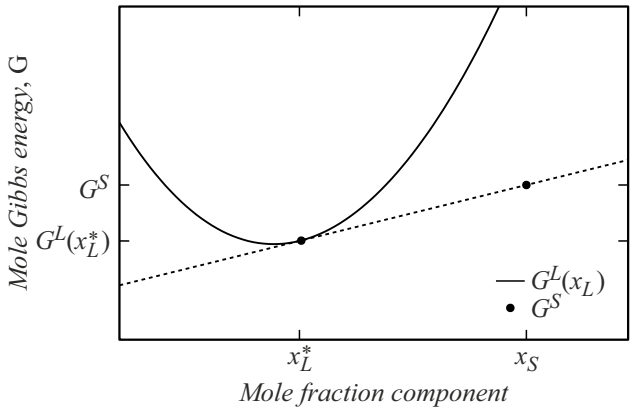

Figure 1. Model Gibbs energies of a phase of variable composition (parabola) and a stoichiometry (dot) with a phase equilibrium line.

energy of the stoichiometry. Figure 1 shows the model Gibbs energies of the stoichiometry (dot) and the phase of variable composition (parabolic function) and intersecting and tangent lines, respectively. To determine the inclination of the line, one may find the ratio between the differences in ordinates and abscissas of two points; at the same time, the inclination of the tangent to the Gibbs energy of the phase of variable composition at the point of contact is $\mu_L(x_L^*)$. The angle may be expressed as

$$k=\mu_L(x_L^*)=\frac{G^S-G^L(x_L^*)}{x_S-x_L^*}.$$

It is evident that the obtained expression corresponds exactly to a thermodynamic source in the case of its zeroing. Thus, the thermodynamic source is zero under the condition of phase equilibrium $\dot\varphi=0$, and the second part of the equation should also be equal to zero: $\sigma^2\nabla\varphi^2-Wg'=0$.

In the one-dimensional case, the remaining part of the equation specifies a stationary solution for the phase field in the form of a „kink" function [16]:

$$\varphi(z)=\frac{1}{2}\big(1-\tanh(z/\delta)\big),$$

where δ is the interface thickness and z is the coordinate. Kinetic coefficient σ^2 and energy barrier height W are related to each other and to physical parameters δ and χ (surface energy density) in the following way:

$$\sigma^2=3\chi\delta,\quad W=\frac{6\chi}{\delta}.$$

The equation for the mole fraction of impurity in the liquid phase is a modified diffusion equation with a source at the interface. To obtain a better estimate, we substitute $\dot\varphi$ with the corresponding equation for the phase field and assume that the „kink" profile is preserved; the pair of terms $\sigma^2\nabla^2\varphi-Wg'$ then adds up to zero. The thermodynamic source may be written as $-p'\Delta\Omega$, where $\Delta\Omega$ is the

thermodynamic force of the phase transition. The equation for the mole fraction then takes the form

$$(1-p)\dot{x}_L = \nabla \cdot \mathbf{J}_D + (p')^2(x_S - x_L)M_\varphi \Delta\Omega.$$

Let us consider the conditions under which the source inside the diffuse boundary is zeroed out. There are two clear cases: when the mole fraction of the liquid phase matches the mole fraction of the stoichiometry and when the thermodynamic source is zeroed out.

The first case may be associated with congruent solidification and melting. In this scenario, x_L is equal or close to x_S, which implies front movement without composition change. Indeed, if one sets the initial distribution of the mole fraction to $x_L(\mathbf{r}, 0) = x_S$, both terms in the diffusion equation vanish. In this case, the dynamics of the system is governed entirely by the phase field equation; therefore, the value and order of magnitude of mobility M_φ determine the velocity of the phase transition front. The model has no restrictions for such scenarios, which means that M_φ may be chosen in such a way as to provide the required dynamics of melting and solidification of a phase of constant composition. The above mechanism may be denoted as a kinetic one.

If $\Delta\Omega = 0$, the entire subsequent dynamics is governed by diffusion flux $\mathbf{J}_D$. The release or absorption of impurity in the region of the interface will continue when the mole fraction shifts away from the equilibrium value. This mechanism of growth or dissolution of a phase of constant composition may be denoted as „diffusion-controlled“ one. The phase transition process is indeed controlled by diffusion in this case, which means that the rate of diffusion processes exceeds the front velocity.

The theoretical approach with separate diffusion-controlled and kinetic mechanisms was considered in [12] (albeit in the vicinity of the liquidus line).

The above reasoning suggests that phase field mobility M_φ depends explicitly on the mole fraction of the phase of variable composition, contradicting the general assumptions of its dependence on temperature only. A functional dependence of this kind may contain a term associated with a sharp peak in the region of the mole fraction of stoichiometry. This approach may provide an explanation for switching of the solidification mechanism from diffusion-controlled to kinetic and back in passing through the $x_L = x_S$ point. This effect may be observed in a numerical experiment by setting such parameters of the functional dependence of M_φ that ensure, on the one hand, thermodynamic consistency in the diffusion-controlled mechanism and, on the other hand, a sharp increase in velocity of the crystallization front in the kinetic mechanism. However, it is currently impossible to test it without actual experiments.

3. Numerical model

To verify the obtained model, we perform numerical simulation in the scenario of directional solidification. For simplicity (specifically, to exclude the effects of surface tension), we consider the one-dimensional case. The mobilities are assumed to be constant: $M_\varphi = \text{const}$ and $M_F = \text{const}$.

Let us reduce system of equations (6) to dimensionless form by introducing substitutions for space and time in the form of $z = \delta\xi$ and $t = t_0\tau$, respectively:

$$\begin{cases} \partial_\tau \varphi = \alpha\left[\partial^2_{\xi\xi}\varphi - 2g' - p'\tilde{G}_0(\overline{G}^S - \overline{G}^L - (x_S - x_L)\overline{\mu}^L)\right], \\ (1-p)\partial_\tau x_L = -(x_S - x_L)p'\partial_\tau\varphi + \partial_\xi\left[(1-p)\partial_\xi\overline{\mu}^L\right], \end{cases}$$

where

$$\partial_\tau = \frac{\partial}{\partial\tau}, \quad \partial_\xi = \frac{\partial}{\partial\xi}, \quad \partial^2_{\xi\xi} = \frac{\partial^2}{\partial\xi},$$

$$\overline{G}^{S,L} = \frac{G^{S,L}}{G_0}, \quad \overline{\mu}^L = \frac{\mu^L}{G_0}, \quad \tilde{G}_0 = \frac{G_0\delta^2}{\sigma^2},$$

$$t_0 = \frac{\delta^2}{M_F G_0}, \quad \alpha = \frac{M_\varphi\sigma^2}{M_F G_0}.$$

Diffusion processes are dominant ($\alpha < 1$) in the resulting dimensionless model. This choice was made on the grounds of practical relevance. It is obvious that the diffusion-controlled mechanism of melting or solidification should prevail in the overwhelming majority of cases (where $x_L(z, 0) \neq x_S$). In the cases with a congruent solidification mechanism (governed by the phase transition kinetics), we raise the value of α by several orders of magnitude ($\alpha \gg 1$) to preserve dimensional time parameter t_0, compensating for this by reducing $\Delta\tau$ to maintain stability.

Let us use the explicit finite difference scheme to solve the obtained dimensionless system. We consider the problem on the $\xi \in [-25; 25]$ interval with initial and boundary conditions

$$\varphi(\xi, 0) = \frac{1}{2}\left(1 - \tanh(\xi)\right), \quad x_L(\xi, 0) = x_0,$$

$$\varphi(-25, \tau) = 1, \quad \varphi(25, \tau) = 0,$$

$$\left.\frac{\partial x_L(\xi, \tau)}{\partial\xi}\right|_{\xi=-25} = \left.\frac{\partial x_L(\xi, \tau)}{\partial\xi}\right|_{\xi=25} = 0.$$

Space step $\Delta\xi = 0.1$ and time step $\Delta\tau$ are chosen empirically with regard to stability of the explicit scheme. Since the solution of the concentration field equation is ambiguous at $\varphi = 1$, we supplement the numerical algorithm with a solution in the form of $x'_L(\xi) = 0$ at $1 - p(\varphi) < 10^{-6}$.

4. Numerical modeling of the process

Let us verify the obtained model by performing numerical modeling for the Si–Ti binary system. One intriguing feature of this system is the existence of two nearby stoichiometric phases: Si_2Ti and SiTi. The other key features of the presented compounds are congruent solidification Liquid $\rightarrow Si_2Ti$ and peritectic reaction Liquid $+ Si_4Ti_5 \rightarrow$ SiTi. Since the model was formulated for two phases, we limit ourselves in peritectics to the interaction of the liquid phase and stoichiometry SiTi. It is evident that the model does not impose any restrictions on the modeled binary system; only the presence of one phase of variable composition (liquid or solid solution) and one stoichiometry is important. Therefore, one may examine an arbitrary system without any features (such as a spinodal or binodal decomposition) instead of Si–Ti.

The following parameters are used for actual modeling: interface thickness $\delta = 10^{-9}$ m, molar volume $V_m = 10^{-6}\,\mathrm{m}^3/\mathrm{mole}$, and $\chi = 0.3\,\mathrm{J/m}^2$.

Figure 2 shows a part of the Si–Ti phase diagram. Points corresponding to the initial conditions of numerical modeling are indicated. Let us consider the diffusion-controlled growth and dissolution mechanism and examine three points (a, a', b) at which the stoichiometric SiTi phase should grow, dissolve, and be in equilibrium with the liquid phase, respectively. We also analyze the kinetic mechanism at points c, c' and verify the possibility of kinetic growth in the „diffusion region“ at points d, d' for the stoichiometric Si_2Ti phase with assumed growth and dissolution in each pair.

The physical conformity of the process is monitored via the equations in dimensionless form, calculation of the total Gibbs energy of system (1), and integration of averaged mole fraction $\langle x \rangle = px_S + (1-p)x_L$ over the entire volume.

Let us consider the diffusion-controlled mechanism of growth and dissolution (a, a', b). In this case, coefficient

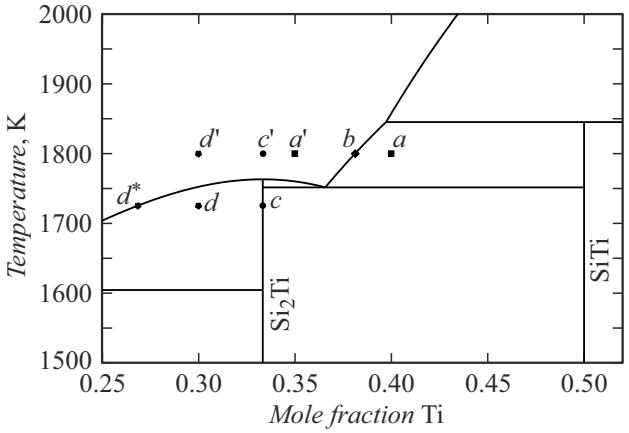

Figure 2. Part of the phase diagram of the Si–Ti binary system with the initial points for numerical modeling indicated, which was plotted with the use of actual experimental Gibbs energies [17].

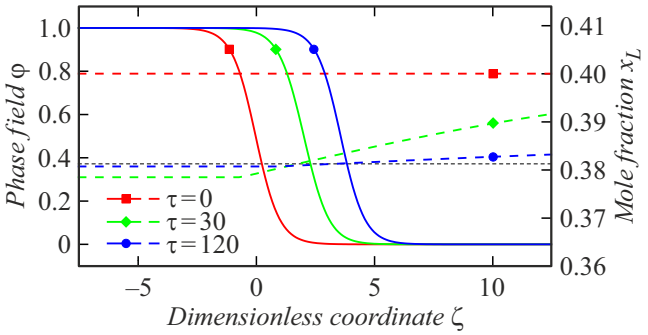

Figure 3. Profiles of phase field φ (solid line) and mole fraction in the liquid phase x_L (dashed line) for the diffusion growth process at different points in dimensionless time.

$\alpha < 1$; we determine empirically the value of this coefficient at which physically acceptable dynamics (specifically, preservation of the interface profile, monotonic non-increase of the Gibbs energy, and preservation of the volumetric amount of impurity) is observed. The results of preliminary modeling demonstrated that the above conditions are satisfied at $\alpha = 0.5$. At smaller values, the pattern remains the same; the only difference is that the front velocity changes. The time step was determined empirically: $\Delta\tau = 10^{-3} = 0.1 \cdot (\Delta\xi)^2$.

The phase field profile (solid line) shifts to the right in Fig. 3, which corresponds to the growth of the stoichiometric phase. The mole fraction in the liquid phase (dashed line) has a clear tendency to slope toward the front where the impurity passes into the solid phase. By the end of modeling, the impurity fraction in the liquid levels out and tends to equilibrium (black dashed line), and the processes subside. It is evident that the mole fraction profile is not entirely correct in the $\varphi \rightarrow 1$ region at intermediate points in time; this behavior is attributable to the specifics of calculation, since the energy and the averaged volume fraction correspond to the underlying physics. One may also notice this profile is normalized by the end of transfer processes. It is worth noting that the geometric symbols on the plots do not denote any significant points and are were added for clarity in black-and-white printing.

The pattern in Fig. 4 is inverse to the one observed in the first case. The profile shifts to the left, indicating dissolution of the stoichiometric phase. The mole fraction profile has a downward trend, suggesting the release and accumulation of impurity in the region of the interface with subsequent transfer to the right boundary. Upon completion of relaxation processes, the mole fraction in the liquid phase tends to the equilibrium value. In the above cases, the fluctuations of relative variation of the averaged impurity mole fraction are on the order of 10^{-6}.

The results of numerical modeling for thermodynamic equilibrium (b) are not shown, since they provide no useful information. As expected, the phase field profile is stationary, and the distribution of impurity in the liquid

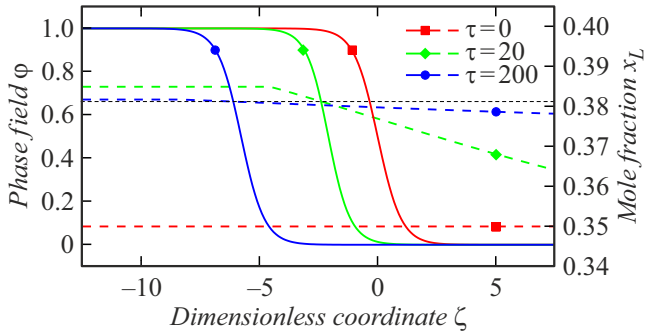

Figure 4. Profiles of phase field φ (solid line) and mole fraction in the liquid phase x_L (dashed line) for the diffusion dissolution process at different points in dimensionless time.

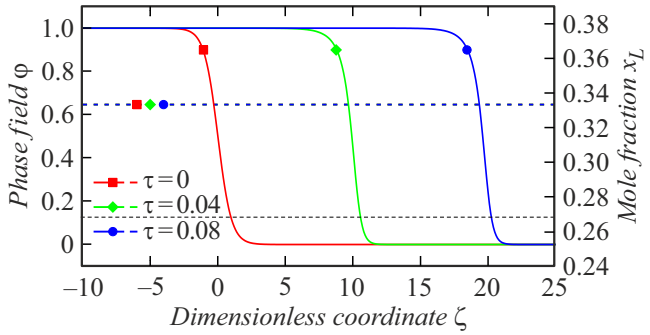

Figure 5. Profiles of phase field φ (solid line) and mole fraction in the liquid phase x_L (dashed line) for the kinetic growth process at $x_0 = x_S$ and different points in dimensionless time.

phase is constant and identical to the initial one. The simulation time was increased by a factor of 2.5 in this case. The relative variation of the averaged fraction is on the order of 10^{-10}.

Let us consider the kinetic mechanism in case c. We set parameter $\alpha = 10^2$ to ensure that the solidification process prevails over the diffusion component. This value is compensated for by time step $\Delta\tau = 10^{-6} = 10^{-4} \cdot (\Delta\xi)^2$ to preserve t_0. The modeling results are presented in Fig. 5. The growth of the stoichiometric phase without compositional changes in the liquid phase is observed. The profile has a curved shape and differs from the stationary solution, but it does not change over time, indicating a different state of local equilibrium for the phase field. This is likely to be associated with a constantly acting non-zero thermodynamic source in the region of the diffuse boundary, since the x_S value is not equilibrium for it. It is worth noting that the front velocity remains constant, deviating from the diffusion case where this velocity decreases over time. The total energy of the system decreases, and the relative variation of the averaged mole fraction in volume is on the order of 10^{-13}.

The case of dissolution under the same initial conditions and parameters (c' in Fig. 6) is also worth noting. The system has a similar behavior pattern in this case, but the front moves to the left. Notably, the curvature of the diffuse boundary profile is inverted relative to the growth case, implying that the sign of the source affects its shape. The relative variation of the averaged mole fraction in volume is on the order of 10^{-12}.

Let us consider case d under the assumption of kinetic solidification. The modeling parameters are the same as in the previous case. A highly atypical pattern is seen in Fig. 7. The front starts moving, and a bulge, which eventually forms a „step," emerges approximately at the level of $\varphi = 0.5$ after a very short time.

This behavior is very much out of line with the dominant paradigm of the phase field method; the values within the phases must be preserved, and they are equal to $\varphi = 0, 1$ in this model. It may be interpreted as the coexistence of two phases in a certain relation. The x_L mole fraction distributions feature a dip that gets deeper with time. This is indicative of rapid consumption of impurity, which is characteristic of the stoichiometry growth process; however, such consumption in the diffuse region is clearly localized closer to the solid phase. The consumption in the liquid phase region is much weaker, and the Fickian flux cannot compensate for the resulting dip, which was noted earlier in the discussion of the kinetic mechanism. It may also be noted that the impurity consumption jumps over the equilibrium value and goes further, tending to zero mole fraction. Chemical potential μ_L has a peculiarity at the

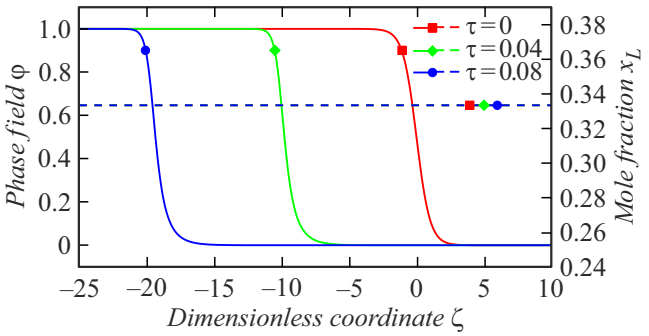

Figure 6. Profiles of phase field φ (solid line) and mole fraction in the liquid phase x_L (dashed line) for the kinetic dissolution process at $x_0 = x_S$ and different points in dimensionless time.

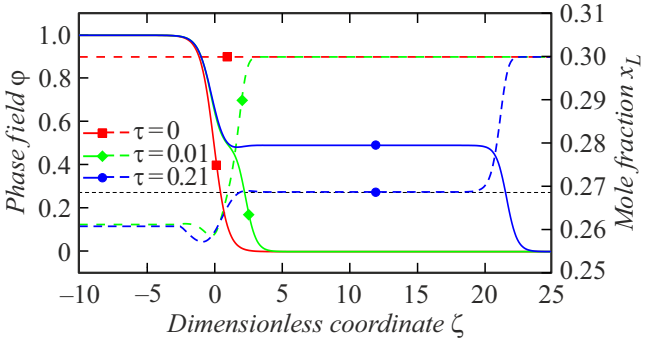

Figure 7. Profiles of phase field φ and mole fraction in the liquid phase x_L for the kinetic growth process at $x_0 \neq x_S$ and different points in dimensionless time.

edges of the mole fraction range: it tends to infinity, sending to infinity the thermodynamic source in the phase field equation (although only in the left part of the diffuse boundary). This instability leads to splitting of the phase field in an attempt to balance the driving force with account for the expression for the averaged mole fraction (the law of conservation of impurity). The system implements the required dynamics through a combination of phases that suppresses the thermodynamic source. The profile of the fraction demonstrates that the steady-state solution is extremely close to the equilibrium value (point (d^*) in the phase diagram). For its part, the energy of the system decreases, and the relative variation of the averaged mole fraction in volume is on the order of 10^{-6}, indicating that the underlying physical principles function correctly. Such behavior may also be interpreted as thermodynamic inconsistency of processes. Another explanation for this effect lies in the isothermal nature of the problem; there is currently no understanding how the system would behave with heat release in the interface since a non-isothermal system of equations would have an extremely nonlinear character.

The dissolution process in case d' (Fig. 8) is analyzed in a similar fashion. In contrast to the previous simulation, the process proceeds correctly with consistent movement of the diffuse boundary to the left. The key feature of this case is the rise of the impurity mole fraction to x_S and subsequent transition to case of c, which is rather unexpected. Presumably, the system tries to nullify the source in the diffusion equation, and since such temperature has no corresponding value of equilibrium mole fraction x_L^* that would zero out the thermodynamic source, zeroing proceeds through the kinetic component.

Figure 9 illustrates the variation of the total Gibbs energy of the system (relative to its initial value) with different ratios of kinetic coefficients as a function of dimensionless time. In cases a and a', the curves are of a relaxation type with asymptotics, which is consistent with the observed dynamics. In case b, the energy is almost constant, but certain fluctuations (on the order of 10^{-3}), which include those in the positive direction, are visible under sufficient magnification. This is presumed to be related to a computational error, and the magnitude of these fluctuations is insignificant. Cases c, c' and d' are characterized by a linear reduction without any inflections and a definite end. The phase field profile does indeed reveal a trend toward infinite motion. Of particular note is case d' where the system undergoes kinetic dissolution in spite of the fact that the point belongs to the „diffusion-controlled region“ (owing to this, the line of relative variation of the Gibbs energy goes near c and c').

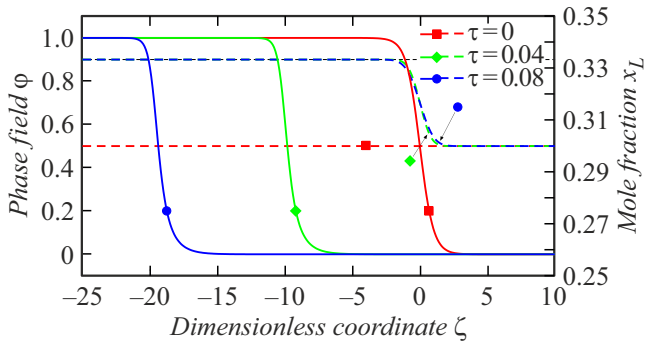

Figure 8. Profiles of phase field φ (solid line) and mole fraction in the liquid phase x_L (dashed line) for the kinetic dissolution process at $x_0 \neq x_S$ and different points in dimensionless time. The black dashed line corresponds to mole fraction x_S.

Case d is characterized by a monotonic energy reduction, although one may notice a dip characteristic of the diffusion-controlled mechanism at the very beginning. This feature differs from the sharp decrease in d'. The obtained profiles make it clear that the phase field splits approximately at $\tau = 0.015$, and the system switches to the kinetic mechanism; from this point on, the plot of relative energy variation resembles a linear one. However, its decrement is significantly less profound than that of similar ones, since the mole fraction of impurity in the „step“ region becomes close to an equilibrium one in the event of phase field splitting, which implies that the thermodynamic source magnitude is smaller than the corresponding value at constant $x_L(\xi, \tau) = x_S$. Therefore, the velocity of the front governed by $\dot{\varphi}$ is significantly lower, and the Gibbs energy reduction is thus also less profound.

In addition to the Si–Ti binary system, systems Cu–Sn, Al–Y, and Al–Co were modeled numerically. Identical results verifying the conclusions made for Si–Ti were obtained in all cases.

5. Numerical modeling of dissolution of graphite in liquid iron

To compare the obtained model with experimental data, we consider the interaction between a drop of liquid iron solution unsaturated with carbon and a graphite substrate under isothermal conditions [18]. It is evident that an actual experiment of this kind may be characterized as macroscopic, while the obtained model operates with mesoscopic systems. This discrepancy complicates the modeling process significantly, since the characteristic spatial and temporal parameters in a mesoscopic scenario are much smaller than those in a macroscopic one. It is technically difficult to combine phenomena of different scales within one formalism. Therefore, we interpolate the experimental data to mesoscopic scales to verify the obtained model.

Let us consider the system as a one-dimensional problem on an infinite interval with a liquid solution of carbon in iron and a stoichiometric phase (graphite) on the right and left semiaxes, respectively. Treating carbon as an impurity, we make an obvious conclusion that the mole fraction of stoichiometry is $x_S = 1.0$, and the initial mole fraction of carbon in liquid is $x_0 = 0.152$ (converted from a mass fraction of 3.7%). Let us direct the coordinate axis vertically

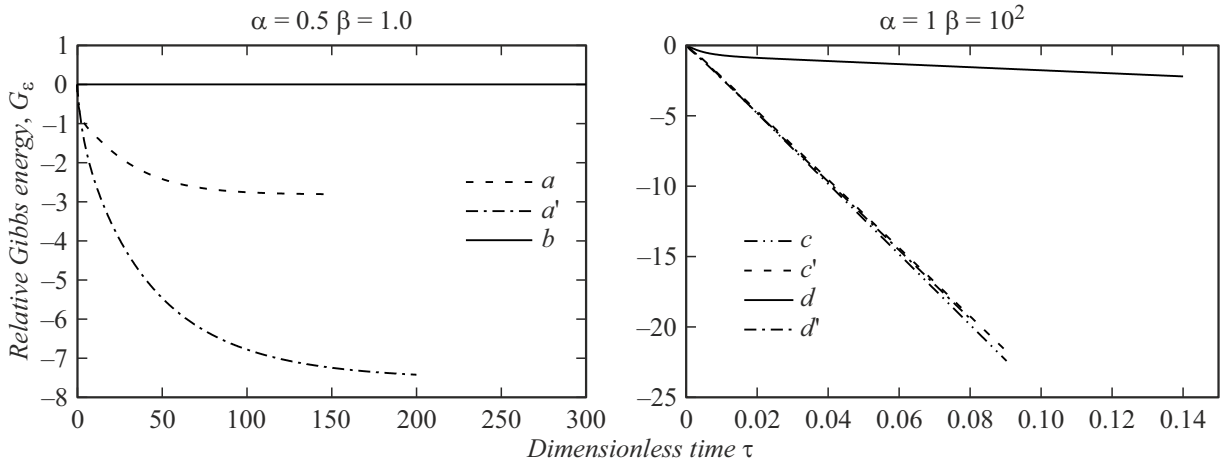

Figure 9. Relative variation of the total Gibbs energy of the system in different cases normalized to the initial energy value.

and perpendicular to the plane of contact between the drop and the graphite substrate. Since the initial fraction of carbon is clearly lower than x_S, we consider a diffusion-controlled dissolution process with coefficients $\alpha = 0.1$ and $\beta = 1$. The molar Gibbs energies of phases were taken from [19].

Since the source of impurity in the liquid phase is confined to the interface, a homogeneous diffusion equation may be examined in the rest of the space. The asymptotic boundary conditions of the third kind, which follow from its solution, are applied at the right boundary. The solution itself is sought (with account for the fact that the diffusion coefficient is equal to unity in dimensionless variables) in the form of Green function

$$x_L(\xi, \tau) = x_0 + A \exp\left(-\frac{(\xi - \xi_0)^2}{4\tau}\right), \qquad (8)$$

where ξ_0 is the position of the phase transition front, which is determined at $\varphi(\xi, \tau) = 0.5$. Differentiating this expression with respect to ξ and expressing A from (8), we obtain

$$\frac{\partial x_L(\xi, \tau)}{\partial \xi} = -\frac{L}{2\tau}\left(x_L(\xi, \tau) - x_0\right), \qquad (9)$$

where L is the distance to the crystallization front. This approach allows one to calculate the mole fraction field at the right boundary with account for asymptotic attenuation at infinity.

Let us consider finite interval $\xi \in [-25; 100]$. When the front reaches coordinate $\xi = -10$, we shift the fields jointly to the right, completing the empty domain with values at the left boundary. Since diffuse boundary width δ in system (7) specifies coefficient $\tilde{G}_0$ of the thermodynamic source and dimensional time parameter t_0 only, we increase it to $\delta = 10^{-8}$ m to reduce the calculation time.

Figure 10 shows the profiles of phase field $\varphi(\xi, \tau)$ and mole fraction $x_L(\xi, \tau)$ in the liquid phase at the moment when $\varphi(-1, \tau) = 0.5$ after two successive shifts. The concentration profiles show signs of operation of boundary

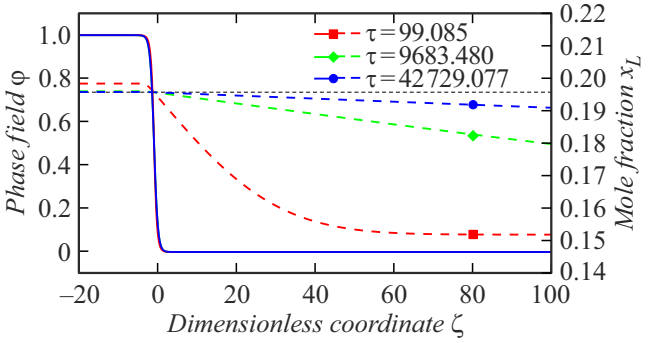

Figure 10. Profiles of phase field φ (solid line) and mole fraction in the liquid phase x_L (dashed line) for isothermal dissolution of carbon in a liquid unsaturated iron solution at different points in dimensionless time τ. The black horizontal dashed line corresponds to the mole fraction of carbon in the liquid phase in the case of phase equilibrium.

conditions of the third kind; the plots „penetrate“ the right boundary of the domain at a non-zero varying angle and are not tied to a specific point (as with boundary conditions of the first kind).

To determine dimensional time, we calculate the specific value of t_0; the Fickian flux mobility may be expressed as

$$M_F = D\left(\frac{d\mu^L}{dx_L}\right)^{-1},$$

then

$$t_0 = \frac{\delta^2}{DG_0}\frac{d\mu^L}{dx_L} = 6.73 \cdot 10^{-8}, \qquad (10)$$

where the value of G_0 and the derivative of the chemical potential were determined at point x_L at which G_L has a minimum. The value of diffusion coefficient D was taken from [20].

Figure 11 (left panel) shows the position of the front (solid line), which is specified by the position of point $\varphi(z, t) = 0.5$, and its velocity (dashed line) as functions of

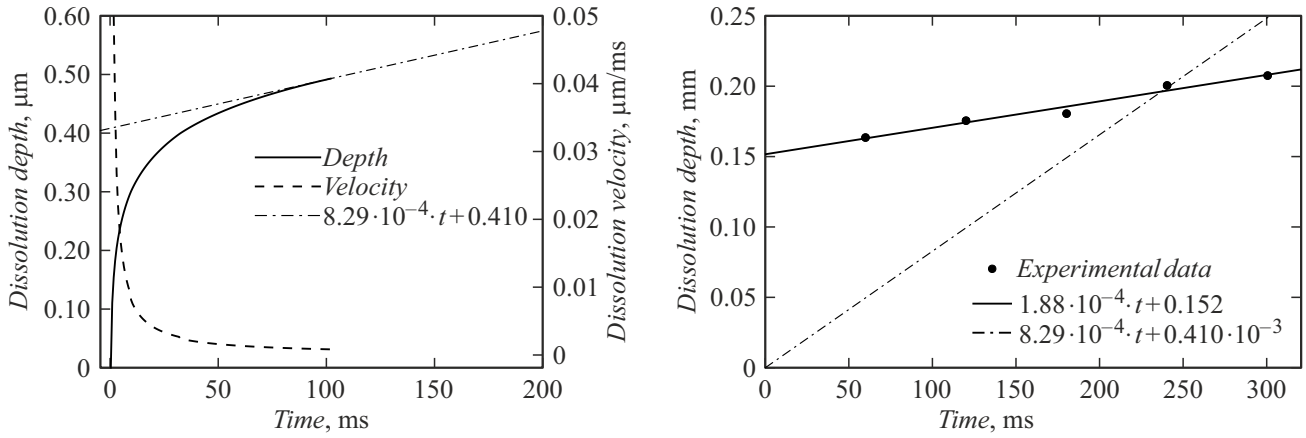

Figure 11. Left panel: plots of the time dependences of graphite dissolution depth (solid line) and rate (dashed line) and the linear function extrapolating the dissolution depth (dash-and-dot line). Right panel: superposition of the obtained linear dependence (dash-and-dot line) and the approximating (solid) line plotted for experimental points [18].

time. It can be seen that the front movement is quite close to being uniform at time $t \approx 80$ ms, which is evidenced by an almost linear time dependence of the front position and a near-constant velocity. However, it is also evident that a certain small contribution, which slows down the front movement and induces deviation of the plots from ideal straight lines, is present in both dependences. Since the problem is solved in an infinite domain, the velocity should obviously tend to zero at $t \to \infty$ (this is a feature of the calculation performed). Let us try to determine the approximate values that the dissolution depth in graphite should reach at times corresponding to the experimental data. With this aim in view, we extend the plot of dissolution depth with a straight (dash-and-dot) line that originates from the end point of modeling with a velocity corresponding to it. In the right panel of Fig. 11, the obtained straight line is contrasted with the experimental data points [19], which are also approximated with a straight (solid) line plotted using the least-squares method. It can be seen that the straight line derived from the numerical experiment does not only match the experimental one in order of magnitude of its values, but also intersects it at an experimental point at $t = 240$ s. Comparing these two linear dependences, one may make two conclusions: the front movement velocity should decrease additionally by a factor of 4.5 and should virtually stop varying at a certain point in time. The plot will then shift upward relative to the abscissa axis, and the dependences will probably match.

Conclusion

A physical and mathematical model of growth and dissolution of a stoichiometric phase in a phase of variable composition (liquid phase) was presented. The obtained model is designed for the simplest case of two-phase interaction within a binary system under isothermal conditions and takes into account the lack of a mathematically defined chemical potential of the stoichiometric phase. The obtained system of equations was analyzed qualitatively, and two mechanisms (namely, diffusion-controlled and kinetic) of phase transition between the stoichiometric phase and the phase of variable composition were identified. Cases corresponding to these two mechanisms and consistent with the physical principles of the process were examined. The model was verified for the Si−Ti binary system with actual experimental Gibbs energies. Profiles of the phase field and the field of mole fraction of impurity in the liquid phase and relative variations of the Gibbs energy and the averaged mole fraction in the growth and dissolution processes were presented.

The results of modeling revealed that the obtained system of dynamic equations based on the principles of thermodynamics coupled with the kinetic law of impurity conservation in volume does not allow for kinetic growth outside a mole fraction close to the stoichiometry value. Splitting of the phase field profile occurs, which violates the dominant paradigm of this method. This leads to a hypothesis that the kinetic mechanism is forbidden thermodynamically and by the conservation law outside the regions of congruent solidification. The only way to confirm or refute this hypothesis is through experiments.

The dissolution of graphite in a liquid iron solution was also simulated in order to verify the obtained model. Since the scales of real-life experiments and the obtained model differ, calculations were performed with the approximations of an infinite domain and boundary conditions of the third kind, which allow one to carry out such calculations on a finite interval. An estimate of the graphite dissolution depth as a function of time was obtained as a result. The plotted dependence is close to the experimental points and matches the actual values in order of magnitude. These results provide, on the one hand, rather crude and, on the other hand, quite compelling evidence in favor of validity of the model and its accuracy in comparison with real objects.

The discussed model may serve as a basis for predictive simulation of the microstructure of alloys containing stoichiometric inclusions in real-world systems. The obtained results of numerical modeling provide a theoretical interpretation of certain phenomena observed in growth and dissolution of stoichiometric phases, may turn out to be crucial for understanding the processes of structure formation in multiphase and multicomponent systems, and also allow one to introduce various physical effects such as surface energy anisotropy (dendritic growth), convection fluxes, processes associated with mechanical stresses, etc., into the studied systems.

Conflict of interest

The authors declare that they have no conflict of interest.

References

[1] V.V. Myl'nikov, A.I. Pronin, M.V. Myl'nikova, E.A. Romanova. Tech. Phys., **68** (1), 26 (2023). DOI: 10.21883/TP.2023.01.55436.218-22
[2] D.M. Herlach, P.K. Galenko, D. Holland-Moritz. *Metastable Solids from Undercooled Melts* (Elsevier, Amsterdam, 2007)
[3] R. Naraghi, M. Selleby, J. Ågren. Calphad, **46**, 148 (2014). DOI: 10.1016/j.calphad.2014.03.004
[4] Y. Zheng, F. Wang, C. Li, J. Cheng, Y. Li. Mater. Sci. Engineer. A, **715**, 194 (2018). DOI: 10.1016/j.msea.2018.01.001
[5] J.E. Spinelli, M.V. Canté, N. Cheung, N. Mangelinck-Noël, A. Garcia. Mater. Sci. Forum, **636–637**, 465 (2010). DOI: 10.4028/www.scientific.net/msf.636-637.465
[6] A. Roy, A. Luktuke, N. Chawla, K. Ankit. J. Electronic Mater., **51** (7), 4063 (2022). DOI: 10.1007/s11664-022-09643-2
[7] A. Kunwar, J. Hektor, S. Nomoto, Y.A. Coutinho, N. Moelans. Intern. J. Mechan. Sci., **184**, 105843 (2020). DOI: 10.1016/j.ijmecsci.2020.105843
[8] V.I. Lad'yanov, S.G. Men'shikova, A.L. Bel'tyukov, B.B. Maslov. Bull. Russ. Acad. Sci. Phys., **74**, 1176 (2010). DOI: 10.3103/S1062873810080423
[9] LVMFlowCV — NovaFlow & SolidCV. — URL: https://lvmflow.ru/ (date of app 07.03.2024).
[10] M. Hillert. *Phase Equilibria. Phase Diagrams and Phase Transformations* (Cambridge University Press, NY., 2008)
[11] S.Y. Hu, J. Murray, H. Weiland, Z.K. Liu, L.Q. Chen. Calphad, **31** (2), 303 (2007). DOI: 10.1016/j.calphad.2006.08.005
[12] H. Miura. Phys. Rev. E, **98**, 023311 (2018). DOI: 10.1103/PhysRevE.98.023311
[13] V.G. Lebedev. JETF Lett., **115** (4), 226 (2022). DOI: 10.1134/S0021364022040075
[14] D. Kessler. J. of Crystal Growth, **224** (1−2), 175 (2001). DOI: 10.1016/S0022-0248(01)00814-4
[15] D. Jou, J. Casas-Vázquez, G. Lebon *Extended Irreversible Thermodynamics* (Springer, NY., 2010)
[16] A.A. Wheeler, W.J. Boettinger, G.B. McFadden. Phys. Rev. A, **45** (10), 7424 (1992). DOI: 10.1103/PhysRevA.45.7424
[17] I. Ansara. *Definition of Thermochemical and Thermophysical Properties to Provide a Database for the Development of New Light Alloys:* COST 507. Vol. 2: Thermochemical Database for Light Metal Alloys (Publ. of the Europ. Communities, Luxembourg, 1998)
[18] C.S. Nguyen, K. Ohno, T. Maeda, K. Kunitomo. ISIJ International, **57** (9), 1491, (2017). DOI: 10.2355/isijinternational.ISIJINT-2017-054
[19] P. Gustafson. Scandinavian J. Metallurgy, **14**, 159, (1985).
[20] D. Goldberg, G.R. Belton. Metall Trans, **5** (7), 1643, (1974). DOI: 10.1007/BF02646337

Translated by D.Safin